

# Room temperature continuous wave THz frequency comb based on quantum cascade lasers

M. Razeghi <sup>a)</sup>, Q. Y. Lu, F. H. Wang, D. H. Wu, and S. Slivken

Center for Quantum Devices, Department of Electrical Engineering and Computer Science,  
Northwestern University, Evanston, Illinois 60208

## ABSTRACT

Frequency combs, spectra of phase-coherent equidistant lines, have revolutionized time and frequency metrology. The recently developed quantum cascade laser (QCL) comb has exhibits great potential with high power and broadband spectrum. However, in the terahertz (THz) range, cryogenic cooling has to be applied for THz QCL combs. We report a room temperature THz frequency comb at 3.0 THz based on difference-frequency generation from a mid-IR QCL comb. A largely detuned distributed-feedback grating is integrated into the QCL cavity to provide the single mode operation as well as enhanced spatial hole-burning effect for multimode comb operation. Multiheterodyne spectroscopy with multiple equally spaced lines by beating it with a reference Fabry-Pérot comb confirms the THz comb operation. This type of THz comb provides a new solution to chip-based high-speed high-resolution THz spectroscopy with compact size at room temperature.

**Keywords:** frequency comb, quantum cascade lasers, group velocity dispersion, four-wave mixing

## 1. INTRODUCTION

Quantum cascade lasers (QCLs) has been becoming the leading mid-IR laser sources thanks to its dramatic advance in power efficiency and widely tailorable frequency emission.<sup>1</sup> Owing to its unique intersubband transition and fast longitudinal phonon scattering, the gain recovery time of a QCL is much shorter than the photon roundtrip time in the cavity. This makes the mode locking very challenging for QCLs.<sup>2</sup> On the other hand, the ultrafast gain recovery time prevents the carrier diffusion from washing away the population grating formed by the spatial hole burning effect, makes the gain no longer clamped by the primary lasing modes and permits new modes to lase resulting multimode operation. Under engineered dispersion and gain profiles, this multimode operation is able to be locked into comb modes with well-defined phase relation via a train of four-wave mixing (FWM) enabled by a third-order  $\chi^{(3)}$  nonlinearity.<sup>3</sup> With the significant development in power efficiency<sup>4,5</sup> and dispersion management<sup>6,7</sup>, frequency comb sources based on mid-IR QCLs have emerged as appealing comb sources in the mid-IR wavelength range with stable phase relation<sup>8</sup>. Based on the same nonlinear effects, QCL frequency comb's operating frequency was also extended to THz range.<sup>9,10</sup> Despite of their potential applications, the development is not yet comparable to its mid-IR counterpart due to its fundamental limitation of cryogenic operation condition.

---

<sup>a)</sup> email: razeghi@ececs.northwestern.edu

Here, we report a room temperature THz frequency comb based on difference-frequency generation from a mid-IR QCL. A largely frequency-detuned distributed-feedback (DFB) grating with respect to the gain peak is integrated into the QCL cavity to provide the single mode operation at  $\lambda_1$  as well as the harmonic-state comb operation at  $\lambda_2$ .<sup>11</sup> The THz comb signal is intracavity generated via down-converting the multimode comb with the DFB mode into the THz range. The device emits in a harmonic state frequency comb with a frequency spacing of 157 GHz in a frequency range of 2.2-3.3 THz and continuous wave power of 5  $\mu$  W at room temperature. This type of THz comb provides a new solution to chip-based high-speed high-resolution THz spectroscopy with a compact size at room temperature.

## 2. DISPERSION MANAGEMENT

The QCL active region was engineered with high nonlinear susceptibilities for THz difference-frequency generation (DFG).<sup>12</sup> To down-converting a mid-IR comb to THz range, a single mode or another mid-IR comb with a different frequency must be pumped simultaneously, as has been done externally using two separate laser sources.

Since the dual wavelength operation with a THz frequency spacing is not easy to achieve in QCLs due to gain competition<sup>13</sup>, many wavelength selection mechanisms are used, including composite DFB<sup>14</sup> and dual-section DFB<sup>15</sup> for single mode THz emissions, multi-section DBR-SGDFB (SG: sampled grating)<sup>16</sup>, dual-section DBR-DFB (DBR: distributed-Bragg reflector)<sup>17</sup> for tunable THz emissions, and weakly-coupled DFB for broadband THz emission<sup>18</sup>. However, none of these techniques can emit a comb and single mode at the same time. This is because DFB structure not only turns to destroy comb operation with strong distributed feedback mechanism for single mode operation, but also introduces a pronounced dispersion which alters the cavity dispersion completely.

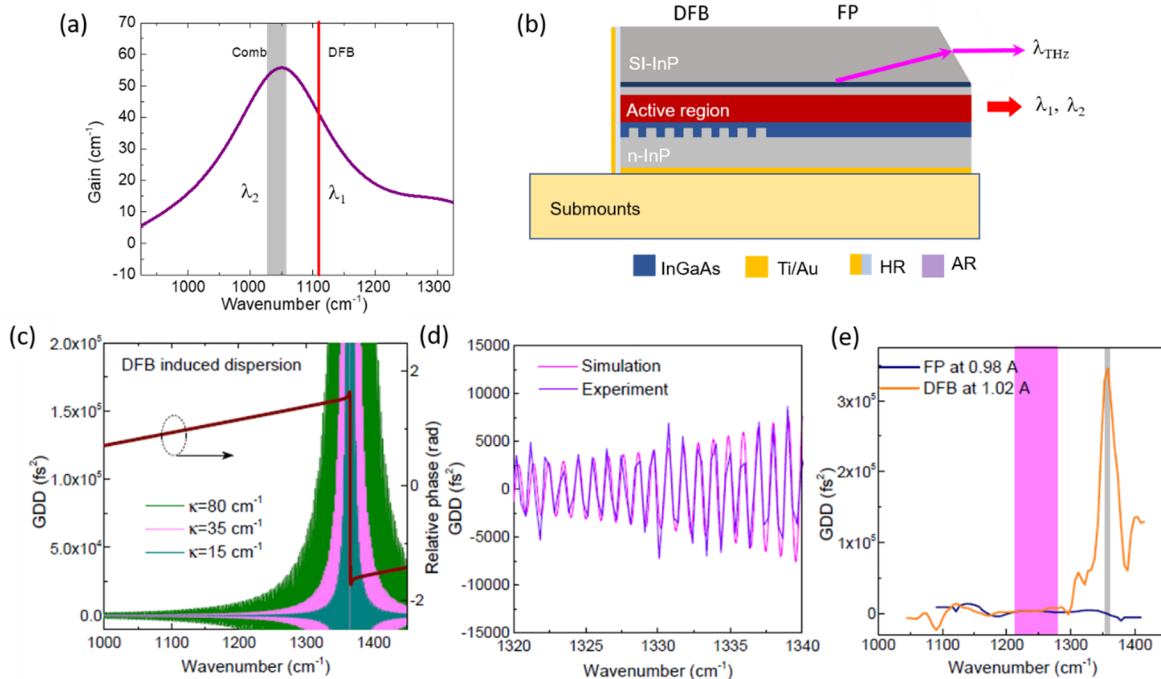


Fig. 1. (a) The relative positions of the DFB and comb wavelengths with respect to the calculated gain spectrum. (b) Schematic of largely detuned DFB QCL design for THz frequency comb operation. (c) Calculated GDD spectra at different coupling coefficient  $\kappa$  and the DFB induced relative phase spectrum for  $\kappa=15$  cm<sup>-1</sup>. (d) Measured high-resolution GDD spectra of a DFB with  $\kappa=35$  cm<sup>-1</sup> and  $L=1.5$  mm and its comparison with the calculated results. (E) Measured low-resolution GDD spectra of the DFB and FP devices. The gray and pink bars indicate grating and comb spectral positions.

A typical DFB grating that is usually used for single mode operation is systematically investigated theoretically and experimentally in Figure 1. The relative phase and group delay dispersion (GDD) of a DFB grating in the QCL-based device as shown in Fig. 1(c). The grating exhibits an abrupt change in relative phase  $\Delta\varphi$  with  $\Delta\varphi \approx \pi$  and a shape dispersion peak at the grating Bragg wavelength. The DFB induced dispersion is highly oscillatory with the repetition frequency determined by the length of grating section. This is confirmed experimentally by the measured high-resolution dispersion transformed from the interferogram of the subthreshold spontaneous spectrum, as shown in Fig. 1(e) and Figure 2. Clearly, this oscillatory feature could completely change the laser cavity dispersion if it was designed at or near the gain peak as in most of the previous DFB designs used for THz generation. Nevertheless, the DFB induced dispersion decreases as the detuning from the Bragg wavelength increases and as the lowering of the grating coupling coefficient  $\kappa$ .

Here, a largely detuned DFB grating is proposed to realize single mode and comb operation in the same cavity. The DFB wavelength position is detuned by  $\sim 80\text{-}90\text{ cm}^{-1}$  with respect to the comb emission wavelength as shown in Figure 1(a). Meanwhile, the grating coupling strength ( $\kappa L$ ,  $L$ = grating length) is set to be 3-5 to secure the single mode operation for the largely detuned DFB design. In the comb operating spectral range of  $1240\text{-}1280\text{ cm}^{-1}$ , the calculated DFB dispersion is limited to  $\pm 1500\text{ fs}^2$ . A low-resolution dispersion analysis was performed for the DFB and a reference Fabry-Pérot (FP) laser with an identical geometry to retrieve the total dispersions of the devices. Similar dispersions of  $\sim 3000\text{ fs}^2$  in the comb operating range were observed for both devices. This reveals that limited dispersions are induced for the designed DFB device near the gain peak, which indicates the grating design will not pose a negative effect on the four-wave mixing for comb operation.

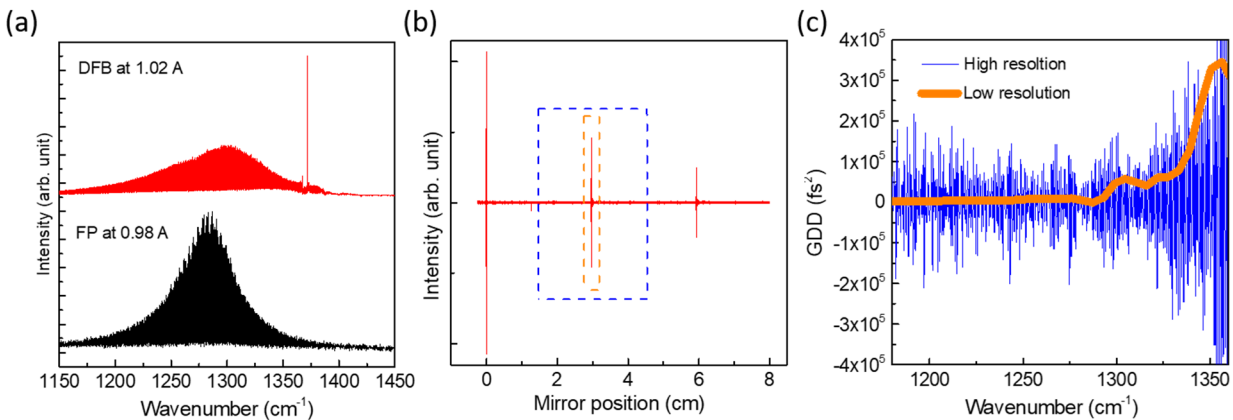


Fig. 2. (a) Measured subthreshold emission spectra for the DFB and FP devices. (b) Interferogram for the DFB spectra. The blue and orange boxes indicate the truncated mirror positions for high- and low-resolution Fourier transforms. (c) Generated high and low resolution GDD spectra. The high-resolution spectrum contains the high-frequency information with a much higher noise level than the low-resolution spectrum.

The DFB and FP devices with the identical geometry are tested using a Bruker Fourier transform infrared (FTIR) spectrometer. The FP device goes through different lasing states, from single mode, to harmonic state, hybrid harmonic-density state, and eventually density state comb operation with a mode spacing defined by one free spectral range (FSR) of the cavity. Narrow beatnote spectra were observed for the FP device with dense-state emissions in a current range  $I=1.42\text{-}$

1.55 A with linewidths <1 kHz. On the contrary, the DFB device emits a single mode at  $\lambda_1=7.25 \mu\text{m}$  defined by the grating period and a pronounced multimode emission at  $\lambda_2=7.81 \mu\text{m}$  simultaneously, as shown in Fig. 3(a). Instead of emitting dense-state fundamental comb as the FP device, the detuned DFB device produces stable multimode emissions with a mode spacing corresponding to 14 times the free spectral range (FSR) of the laser cavity for currents  $I \leq 1.5 \text{ A}$  and 22 times the FSR at higher currents. This shows the device skips many longitudinal modes and favors a few, powerful modes separated by many FSRs.

The single mode emission resulted from the DFB section forms a spatial population grating in the cavity and induces an incoherent gain for multimode operation near the gain peak at higher currents. On the other hand, the beating between the single mode and the multimode introduces additional population pulsation nonlinearity which in turn contributes to the mode skipping of the multimode emission in the working current range.

This harmonic comb phenomenon has also been recently observed from QCLs with different coating conditions at different wavelengths<sup>19,23</sup>, which indicates the underlying mechanism is an intrinsic property of QCLs, i.e. the fast gain recovery time associated with the intersubband transition. However, the operation range of harmonic comb is limited in narrow current ranges. The harmonic comb can be enhanced by increasing the asymmetry of the cavity with HR-AR coating to weaken the population grating effect and force the device undergo only the AM instability or by pumping the device with an external laser<sup>20</sup>. The detuned DFB design in this work provides another approach to effectively improve the current dynamic range of the comb operation by enhancing the SHB effect and population pulsation effect.

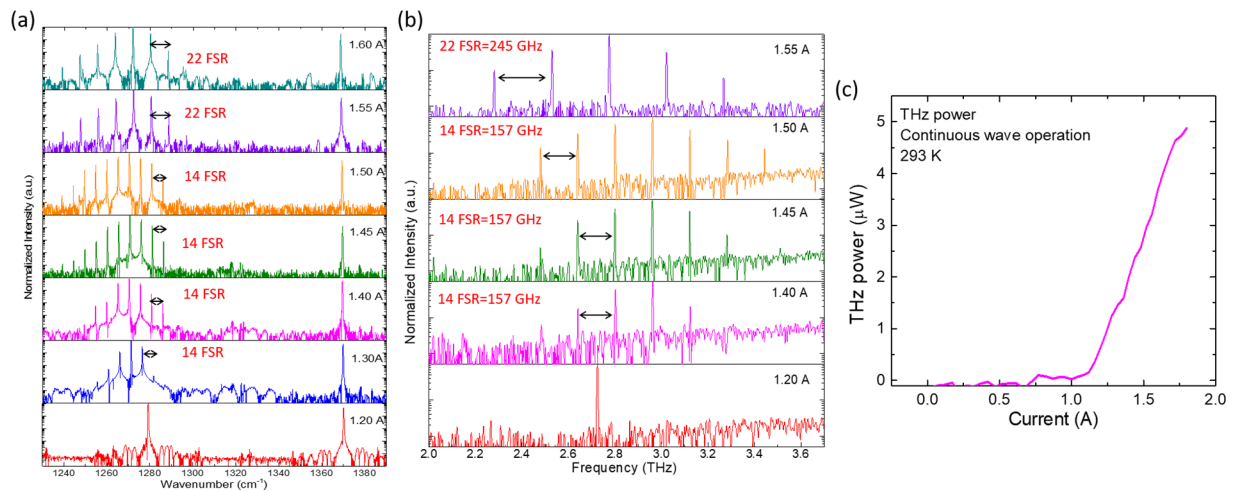


Fig. 3. (a) Lasing mid-IR spectra of the 4-mm long DFB QCL evolving with current at room temperature in continuous wave operation. (b) Lasing THz spectra of the DFB QCL comb evolving at different currents at room temperature continuous wave operation. (c) THz power characterization of the DFB QCL comb at room temperature continuous wave operation.

The dual wavelength operation of the DFB device enables the second-order difference-frequency generation that can transfer the mid-IR comb into the THz range. The SI InP substrate allows extraction of THz radiation through the substrate via the Čerenkov phase matching scheme for broadband THz generation. The THz emitting spectra were measured with the FTIR spectrometer equipped with a silicon bolometer. Multimode harmonic comb operation in the THz range was observed in a wide current range. The mode spacing is 157 GHz for currents between 1.3-1.5 A and 245 GHz for currents >1.5 A. These spacings correspond to 14 FSR and 22 FSR mode spacings determined by the mid-IR pumping

combs. Thanks to the mid-IR harmonic state comb operation with a limited mode number, the converted THz light intensity is concentrated on a limited number of comb modes with a side mode suppression ratio up to 20 dB. The THz power was measured with a calibrated Golay cell detector. The DC injecting current is modulated with a low frequency modulation to match the testing condition of the detector. The DFB device emits a continuous THz power up to 5  $\mu$ W, as shown in Figure 3 (b), which indicates that average power of 1  $\mu$ W for each THz mode is achieved.

Optical power-current-voltage ( $P-I-V$ ) characterizations for both devices under continuous wave operation at 293 K are performed. The DFB device emits a continuous wave power up to 0.46 W with a threshold current density of 2.7 kA/cm<sup>2</sup> as shown in Figure 3 (c), while the FP device emits up to 0.73 W with a threshold current density of 2.5 kA/cm<sup>2</sup>. The slope efficiency is 1.18 W/A, compared to the 0.81 W/A for the DFB device. The reduced slope efficiency of the DFB device compared with the FP device is expected since the FP device, featuring dense-state comb operations at higher currents, is able to extract more gain and power than that of the DFB device.

### 3. HETERODYNE AND OFFSET FREQUENCY TUNING MEASUREMENT

Since the mode spacing of the harmonic state comb with many FSRs exceeds the bandwidth of conventional mid-IR detectors, a multi-heterodyne beating experiment between the harmonic state DFB device and a reference comb device can be performed to assess the comb operation for the DFB device.<sup>21</sup> Here the FP device is biased into a fundamental comb operation regime to serve as the reference comb. The two devices were focused on a high-bandwidth quantum well infrared detector (QWIP) (Bandwidth>20 GHz) for heterodyne measurement and the heterodyne signal was recorded with a spectrum analyzer. In parallel, the beams from the two devices are sent to the FTIR for spectral characterization<sup>22</sup>. For this experiment, the offset frequencies of both devices were tuned with current/temperature to be close to each other by the monitoring the lasing spectra. The FP device was biased at a current of 1.52 A to lase in the fundamental comb state, while the DFB device was biased to 1.45 A to lase in the multimode harmonic state, as shown in Fig. 4(b). The heterodyne spectra were recorded with a spanning range of 5 GHz, a resolution bandwidth (RBW) of 300 kHz, and scan time of 100 ms. Fig. 4(c) shows that equally-spaced beating modes are observed on the multi-heterodyne spectrum with a mode spacing of 580 MHz, corresponding to the beating of the central 7 modes from the DFB device with the FP comb modes. The linewidth for each beat signal is  $\sim$ 300 kHz which is limited by the RBW. The current of the DFB device is then increased steadily to 1.55 A to lase in the harmonic state with a different mode spacing of 22 FSR. The recorded heterodyne spectrum with a mode spacing of 390 MHz is shown in Fig. 4(d). Note that the heterodyne mode spacing is merely determined by the frequency difference between the mode spacing of the harmonic comb and the integer multiple of FP mode spacing. Given the comb operation of the FP device at the biased current, this multi-heterodyne experiment verified the harmonic comb operation of the DFB device.

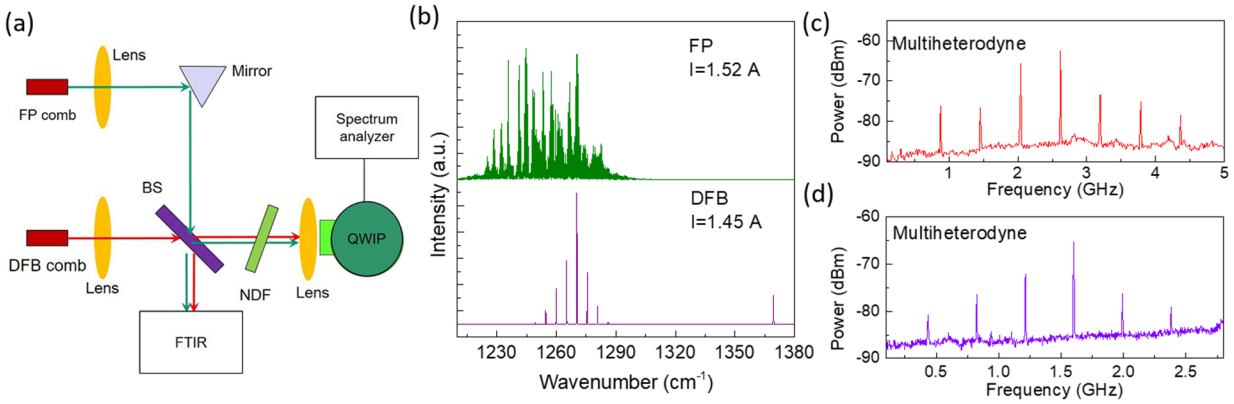


Fig. 4. (a) lasing spectrum in logarithmic scale at 820 mA for the GTI-coated QCL device. (b)  $P$ - $I$ - $V$  characterization of 5-mm long, GTI-coated QCL comb devices in CW operation at 293 K. (c) Scanning electron microscope (SEM) image of the cross section of a typical GTI mirror coated on a QCL-comb back facet. (d) Measured GDD of the GTI-coated QCL device near their threshold current density. (e) Electrical beatnote spectrum at 820 mA. (f) Multi-heterodyne beating of the two combs, corresponding to an optical bandwidth of  $30 \text{ cm}^{-1}$ .

The carrier offset frequency  $f_{ceo,1}$  of the FP QCL comb cannot be precisely determined because the laser is in free-running condition. However, its tuning rate as a function of current or temperature can be determined by comparing the change of the repetition frequency  $f_{rep,1}$  and the lasing frequency  $f_m$ . Figure S3(a) shows the lasing spectra of the FP device at different currents. Given the measured electrical tuning rate of  $-75 \text{ kHz/mA}$ , and  $-4.92 \text{ cm}^{-1}/\text{A}$  for  $f_{rep,1}$  and  $f_m$ , the electrical tuning rate for  $f_{ceo,1}$  is estimated to be  $107 \text{ MHz/mA}$ . This tuning rate of the carrier frequency is also close to that reported in Ref. 23. Clearly, the shift of the offset frequency  $f_{ceo,1}$  is much larger than that of the repetition frequency, this is mainly because the offset frequency tuning is expected to be  $N$  times higher than the repetition frequency tuning, where  $N$  is the number of comb lines. Similarly, consider the measured temperature tuning rate of  $-1.5 \text{ MHz/K}$ , and  $-0.2 \text{ cm}^{-1}/\text{K}$  for  $f_{rep,1}$  and  $f_m$ , the temperature tuning rate for  $f_{ceo,1}$  is estimated to be  $-0.91 \text{ GHz/K}$ .

Since the repetition frequency  $f_{rep,2}$  for the harmonic comb is so large and cannot be measured directly with the spectrum analyser, we will use Eqs. (1-6) to estimate the tuning rate for  $f_{rep,2}$  and  $f_{ceo,2}$ . In the experiment, the bias on the DFB device is fixed while the tuning FP current to tune the heterodyne signal. The corresponding tuning rate for the heterodyne frequency is measured to be  $20 \text{ MHz/mA}$  (Fig. S3(b)). From Eqs. 4-6, a tuning rate of  $-355 \text{ kHz/mA}$  is obtained for  $f_{rep,h}$ . As a result, we induced the repetition tuning rate of  $-1.39 \text{ MHz/mA}$  for harmonic comb  $f_{rep,2}$ , which is determined by:  $f_{rep,2} = f_{rep,h} + (m/n) f_{rep,1}$ . Considering the electrical tuning rate of  $-5.6 \text{ cm}^{-1}/\text{A}$  for the mid-IR harmonic comb, its carrier offset frequency  $f_{ceo,2}$  tuning rate is estimated to be  $173 \text{ MHz/mA}$  from Eq. (2).

For the intracavity generated THz comb, using the measured electrical tuning rate of  $-6.16 \text{ cm}^{-1}/\text{A}$  for the DFB wavelength, with the information of the tuning rates of  $f_{rep,2}$  and  $f_{ceo,2}$  for the harmonic comb, the tuning rates of the emitting frequency and carrier frequency for the THz comb are estimated to be  $-0.56 \text{ cm}^{-1}/\text{A}$  and  $6.9 \text{ MHz/mA}$ . Both parameters are over ten times smaller than the mid-IR comb counterparts. This is attributed to the fact that the two mid-IR pumping sources from the same chip sharing similar frequency tuning rates, which improves the stability of the THz comb.

## 4. CONCLUSIONS AND PERSPECTIVES

The demonstrated largely detuned DFB design enables new features that are extremely useful for mid-IR and THz comb generation. First, it enhances harmonic comb operation with an increased current dynamic range and its reproducibility by introducing strong SHB and population pulsation effects. Pronounced harmonic frequency comb operation has been repeatedly observed from multiple DFB devices. This approach could be further improved to explore monolithic control and tuning of the harmonic comb emission. When the DFB is designed with a wavelength closer to the gain peak and a reduced coupling coefficient  $\kappa$ , the single DFB emission could be used as an optical seeding to control and tune the harmonic comb emission with its injection current provided that the DFB section is electrically isolated from the rest of the cavity. More importantly, the dual wavelength operation of DFB and harmonic comb operation enables chip-based THz comb operation at room temperature without any external optical elements. The next step of our research will be focused on the realization of fundamental THz frequency comb operation by DFG in QCL. This can be achieved by reducing the SHB effect either by reducing the DFB coupling strength or using an anti-reflection coating on the front facet. This will also enable more comb modes to extract gain for higher power operation.

In conclusion, we report a room temperature THz frequency comb at 3.0 THz based on difference-frequency generation from a mid-IR QCL comb. A largely detuned distributed-feedback grating is integrated into the QCL cavity to provide single mode operation as well as an enhanced spatial hole-burning effect for multimode comb operation. The THz comb signal is intracavity generated via down-converting the mid-IR multimode comb with a DFB mode into the THz range spanning 2.2-3.3 THz. This device design not only elucidates new design schemes for the control of the harmonic comb in mid-IR range, but also enables a new type of THz comb that is chip-based at room temperature and is appealing to applications like high-speed communication, spectroscopy, imaging, and astronomical observations.

## 5. ACKNOWLEDGEMENTS

This work is partially supported by the National Science Foundation (grants ECCS-1505409 and ECCS-1607838). The published material represents the position of the author(s) and not necessarily that of the National Science Foundation. The authors would also like to acknowledge the encouragement and support of all the involved program managers.

## REFERENCES

1. Razeghi, M., Lu, Q. Y., Bandyopadhyay, N., Zhou, W., Heydari, D., Bai, Y., & Slivken, S. Quantum cascade lasers: from tool to product. *Opt. Express*, **23**, 8462 (2015).
2. Wang, C. Y. *et al.* Mode-locked pulses from mid-infrared quantum cascade lasers. *Opt. Express* **17**, 12929–12943 (2009).
3. Hugi, A., Villares, G., Blaser, S., Liu, H. C., & Faist, J. Mid-infrared frequency comb based on a quantum cascade laser. *Nature* **492**, 229 (2012).
4. Lu, Q. Y. *et al.* High efficiency quantum cascade laser frequency comb. *Sci. Rep.* **7**, 43806 (2017).
5. Jouy, P. *et al.* Dual comb operation of  $\lambda\sim 8.2$   $\mu\text{m}$  quantum cascade laser frequency comb with 1 W optical power. *Appl. Phys. Lett.* **111**, 141102 (2017).
6. Villares, G. *et al.* Dispersion engineering of quantum cascade laser frequency combs. *Optica* **3**, 252 (2016).

7. Lu, Q. Y., Manna, S., Slivken, S., Wu, D. H., & Razeghi, M. Dispersion compensated mid-infrared quantum cascade laser frequency comb with high power output. *AIP Advances* **7**, 045313 (2017).
8. Singleton, M., Jouy, P., Beck, M. & Faist, J. Evidence of linear chirp in mid-infrared quantum cascade lasers. *Optica* **5**, 948–953 (2018).
9. Burghoff, D. *et al.* Terahertz laser frequency combs. *Nature Photon.* **8**, 462–467 (2014).
10. Rösch, M., Scalari, G., Beck, M., & Faist, J. Octave-spanning semiconductor laser, *Nat. Photonics* **9**, 42–47 (2015).
11. Lu, Q. Y., Wang, F. H., Wu, D. H., Slivken, S., & Razeghi, M. Room temperature terahertz semiconductor frequency comb, *Nature Commun.* **10**, 2403 (2019).
12. Lu, Q. Y., Wu, D. H., Sengupta, S., Slivken, S., & Razeghi, M. Room temperature continuous wave, monolithic tunable THz sources based on highly efficient mid-infrared quantum cascade lasers, *Sci. Rep.* **6**, 23595 (2016).
13. Geiser, M. *et al.* Gain competition in dual wavelength quantum cascade lasers. *Opt. Express* **18**, 9900–9908 (2010).
14. Lu, Q. Y., Bandyopadhyay, N., Slivken, S., Bai, Y., & Razeghi, M. Room temperature single-mode terahertz sources based on intracavity difference- frequency generation in quantum cascade lasers. *Appl. Phys. Lett.* **99**, 131106 (2011).
15. Vijayraghavan, K. *et al.* Broadly tunable terahertz generation in mid-infrared quantum cascade lasers. *Nat. Commun.* **4**, 2021 (2013).
16. Lu, Q. Y., Slivken, S., Bandyopadhyay, N., Bai, Y., & Razeghi, M. Widely tunable room temperature semiconductor terahertz source. *Appl. Phys. Lett.* **105**, 201102 (2014).
17. Jung, S. *et al.* Broadly tunable monolithic room-temperature terahertz quantum cascade laser sources. *Nature Commun.* **5**, 4267 (2014).
18. Fujita, K. *et al.* Ultra-broadband room-temperature terahertz quantum cascade laser sources based on difference frequency generation. *Opt. Express* **24**, 16357-16365 (2016).
19. Lu, Q. Y. *et al.* High power frequency comb based on mid-infrared quantum cascade laser at  $\lambda \sim 9 \mu\text{m}$ . *Appl. Phys. Lett.* **106**, 051105 (2015).
20. Piccardo, M. *et al.* Widely tunable harmonic frequency comb in a quantum cascade laser. *Appl. Phys. Lett.* **113**, 031104 (2018).
21. Kazakov, D. *et al.* Self-starting harmonic frequency comb generation in a quantum cascade laser. *Nat. Photonics* **11**, 789–792 (2017).
22. Lu, Q. Y., Razeghi, M., *et al.* Shortwave quantum cascade laser frequency comb for multi-heterodyne spectroscopy. *Appl. Phys. Lett.* **112**, 141104 (2018).
- 23 Burghoff, D. *et al.* Optomechanical control of quantum cascade laser frequency combs. *Proc. SPIE* **10939**, 109391E-1(2019).